Structural Characterization of Electrooptically Active Poly(nonylbithiazole)

L. González-Ronda and D. C. Martin*

Macromolecular Science and Engineering Center and Department of Materials Science and Engineering, 2022 H. H. Dow Building, The University of Michigan, Ann Arbor, Michigan 48109-2136

J. I. Nanos, J. K. Politis, and M. D. Curtis

Macromolecular Science and Engineering Center and Department of Chemistry, 2807 Chemistry Building, The University of Michigan, Ann Arbor, Michigan 48109-1055

Received January 14, 1999; Revised Manuscript Received April 28, 1999

ABSTRACT: We have examined the microstructure, solution processing, thermal transitions, and mechanical properties of regioregular poly(nonylbithiazole) (PNBT). PNBT can adopt three distinct colors in the solid state—yellow, red, and metallic green—depending on processing conditions such as polymer concentration, solvent evaporation rate, temperature, and pressure. Microstructural variations were observed between samples of different colors, including the intensification of optical absorption with the degree of crystalline order and/or crystal size. Yellow samples lacked well-developed three-dimensional order, whereas red and green samples were semicrystalline. The development of a lyotropic mesophase was observed at intermediate concentrations in a "diffusion couple" geometry. A crystal model with two planar, π-stacked chains per unit cell was shown to be consistent with the experimental diffraction data. The simulated orthorhombic unit cell parameters are $a = 2.38$ nm, $b = 0.72$ nm, and $c = 0.79$ nm.

1. Introduction

Processable conjugated polymers have been a topic of intense research in recent years due to their potential use as the active layers of light-emitting diodes (LEDs),[1] thin-film transistors (TFTs),[2] and chemical sensors.[3] Substituted polythiophenes in particular have received much attention due to their processability and good electrooptical properties. The increased backbone flexibility associated with alkyl substitution has given rise to soluble and fusible materials whose electrooptical properties may vary significantly with temperature,[4] pressure,[5,6] and solvent interactions.[7] These property changes are further affected by variations in side chain length[8−10] and stereoregularity.[10−12]

The structure of polythiophene (PT) is strongly dependent on the nature and length of its substituents. Many studies have thus focused on the effects of different substituent geometries and chemical structures, such as alkoxy chains[13] and nonalternating alkyl chains,[14] on the three-dimensional order of PT. Systematic analyses of the structure of poly(3-alkylthiophene)s (P3ATs) as a function of chain length have revealed a lamellar-like structure in which planar backbones stack on top of each other.[8,15,16] This geometry remains fairly constant for side chains ranging from butyl to hexadecyl, with only minor fluctuations in the $\pi-\pi$ stacking and repeat-unit distances.[8,10,16] The side-to-side or lamellar spacing scales with side chain length as expected, but the relationship deviates from linearity for chains longer than hexyl, presumably due to increasing disorder.[9,17]

Temperature- and solvent-induced changes in the electrooptical properties of P3ATs have been attributed to the formation and localization of chain twist defects known as conformons.[7,18,19,23] Transformations between localized, distributed, and continuous conformons have been proposed by Inganäs and co-workers as the mechanisms for such thermo- and solvatochromatic behavior, in which twists become both more numerous and more delocalized with increasing thermal or solvating energy.[7] The evolution of the electrical properties of unsubstituted PT as a function of conformon localization has been studied by Brédas et al.[20] Their calculations have predicted relatively small changes in the band gap, bandwidth, and ionization potential of PT for torsion angles smaller than 40°. This is consistent with the mechanism proposed by Yang et al. for the thermochromatic transitions of P3ATs, in which gradual changes in chain torsion cause continuous shifts in absorption maxima.[10] In those instances when a mesophase mediated the transition between crystalline and isotropic states, the observed shift in absorption spectra was continuous, whereas direct transitions between crystalline and isotropic states showed a discontinuity in the wavelength of maximum absorption, i.e., an isosbestic point.

Because of the electron-excessive nature of thiophene rings, P3ATs are susceptible to p-doping and insensitive to n-doping. However, the incorporation of an imine nitrogen into the conjugated backbone of substituted polythiophenes has led to the synthesis of n-dopable poly(bithiazole)s,[21,22] which show structure−property relationships similar to those observed in P3ATs.[21,23] Poly(alkylbithiazole)s (PABTs) have been found to have reduction potentials of −1.77 to −2.3 V and to remain stable during repeated doping and dedoping cycles.[23−25] Furthermore, methylation of the imine nitrogen in the nonyl-substituted poly(bithiazole) (PNBT) has been shown to lower the reduction potential of the polymer from −1.93 to −1.38 V and improve its electrical and mechanical properties.[26] The device behavior of LEDs based on N-methylated PNBT and the polymer's ability to serve as an electron injection layer have been evaluated by Curtis and co-workers.[26,27]

In this work, we discuss the microstructure and microstructural changes of PNBT in the context of previous research on P3ATs. PNBT can adopt three

10.1021/ma990057+ CCC: $18.00
Published on Web 06/17/1999

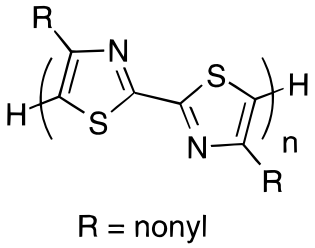

Figure 1. Chemical structure of poly(nonylbithiazole) (PNBT).

distinct solid-state morphologies, each of which shows significantly different electrooptical properties.[21] We have characterized the influence of processing on the optical properties of PNBT and examined the microstructures associated with these changes. The following is a structural analysis based on our optical microscopy, differential scanning calorimetry, X-ray diffraction, electron diffraction, and molecular modeling studies.

2. Experimental Procedure

Synthesis. Stereoregular PNBT (Figure 1) was synthesized by Curtis and co-workers by dehalogenative coupling of 5,5′-dibromo-4,4′-dinonyl-2,2′-bithiazole with nickel in refluxing toluene.[21] Molecular weights of $M_n = 22\,000$ and $M_w = 44\,000$ were measured using gel permeation chromatography against polystyrene standards.

Processing. PNBT is soluble in solvents such as toluene and chloroform.[21] The solutions prepared for this study required high heat and vigorous stirring. Solution stability decreased with increasing polymer concentration; those with concentrations above approximately 0.05 wt % showed signs of polymer precipitation after 1−2 weeks.

PNBT films were made by spin coating and film casting from chloroform and toluene solutions. The choice of solvent and solution concentration was varied to produce samples of different morphologies and thicknesses. For instance, spin coating from dilute solution produced uniform thin films (less than 1 μm) which were used for UV−vis spectroscopy and optical microscopy. On the other hand, films as thick as 20 μm were solvent-cast from solutions of 0.2−1.5 wt % polymer and used in X-ray diffraction studies and tensile tests. This process involved casting the solutions onto glass slides and covering them with a Petri dish to slow the drying process. The dry films were removed after 1−2 days by submerging the coated slides in methanol, a nonsolvent.

Fibers were wet spun from 0.5 wt % polymer solutions of PNBT in either chloroform or toluene. About 1 mL of polymer solution was spun from a needle 6 μm in diameter into a coagulating methanol bath. The wet fibers were not drawn but collected onto a take-up unit as-spun. Additional fibers for electron diffraction analysis were spun using an electrodeposition technique.[28] During this process a 0.5 wt % solution of PNBT in chloroform was spun onto carbon-coated mica sheets by inducing a voltage differential of 8 kV between the 6 μm needle and the target, located 3 cm apart. The coated mica sheets were then annealed in air at 270 °C for approximately 8 h.

Thermal Characterization. The thermal stability of various PNBT specimens was tested using a series 7 Perkin-Elmer thermogravimetric analyzer (TGA). Samples were heated from 25 to 800 °C at a rate of 40 °C/min under both nitrogen and air atmospheres.

The thermal behavior of various PNBT specimens was monitored using a series 7 Perkin-Elmer differential scanning calorimeter (DSC). Specimens with weights of 2−10 mg were subjected to two or more consecutive heating and cooling cycles. Each cycle involved heating the sample from 200 to 310 °C at a rate of 10 °C/min, annealing at 310 °C for 5 min, and cooling to 200 °C at a rate of 10 °C/min. Transition temperatures, heats of fusion, and heats of crystallization were calculated using the DSC 7 software.

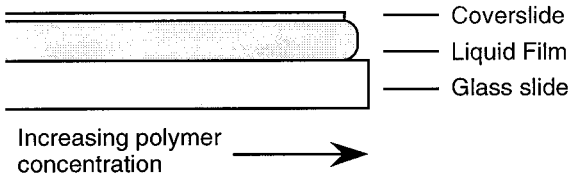

Figure 2. Schematic view of a diffusion couple. Solvent evaporation induces a concentration gradient in the confined polymer solution.

Structural Characterization. Changes in color and molecular order of PNBT solutions, films, and fibers were studied through optical microscopy. The behavior of films and fibers as a function of temperature was analyzed using a Nikon Optiphot 2-Pol microscope, a Linkam TH1500 hot stage, and a Linkam TMS91 programmable temperature controller. Images were recorded with a Sony CCD video camera, digitized with a RasterOps acquisition board in a Macintosh IIci, and analyzed using the public domain software NIH Image (available at http://rsb.info.nih.gov/nih-image/).

The lyotropic behavior of PNBT solutions was examined using a diffusion couple geometry (Figure 2). Small amounts of a 0.5 wt % PNBT solution in chloroform or toluene were confined between a glass slide and a coverslip for examination in the optical microscope. The specimens were placed between crossed polarizers and observed under transmitted light as the solvent evaporated. Gradual solvent evaporation from the edges of the sandwiched specimen created a concentration gradient and allowed the examination of thin and uniform specimens for the presence of liquid crystalline phases at different polymer concentrations.[29,30]

One- and two-dimensional X-ray diffraction data were collected on PNBT films, fibers, and as-synthesized samples. Wide-angle X-ray scattering (WAXS) data were digitally collected on a Rigaku Rotaflex diffractometer operated at 40 kV and 100 mA with a Cu target ($\lambda = 0.154$ nm) and a graphite monochromator. Samples were scanned from 3° to 35° (2θ) at 0.01° intervals and a rate of 1°/min. Small-angle X-ray scattering (SAXS) data were obtained with a Braun position-sensitive detector using a Kratky camera equipped with a fixed tube X-ray source and a Cu target ($\lambda = 0.154$ nm). X-ray patterns of wet-spun PNBT fiber bundles were obtained using a Statton camera attached to the same X-ray source.

Curve fits of the one-dimensional WAXS data were obtained using the software package Igor Pro,[31] using a nonlinear least-squares refinement method. The best results were obtained by fitting crystalline peaks with a Lorentzian function and amorphous peaks with a Gaussian function. The fitted curves were then used to calculate the average crystal dimensions of the samples according to the Scherrer equation.[32] Degrees of crystallinity were calculated using an internal comparison method, which involves calculating the relative areas of the crystalline and amorphous contributions to the diffraction pattern.[32]

Selected area electron diffraction (SAED) fiber patterns were obtained from the electrospun PNBT samples using a JEOL 2000 EX operated at 200 kV. The PNBT-coated carbon film was thermally annealed at 200 °C for 2 h and removed from the mica by submerging the sheets into deionized water and lifting the floating carbon films with 400 mesh copper grids.

Molecular Modeling. The crystal structure of PNBT was modeled using the Cerius[2] Molecular Modeling software package.[33] The initial polymer model was constructed by adding bonds to a model of the known monomer crystal structure, as determined from X-ray diffraction.[21] Energy minimization was performed under triply periodic boundary conditions using the Dreiding 2.21 force field,[34] the default conjugate gradient algorithm, and a gradient convergence criterion of 0.001 kcal/(mol Å). The powder and fiber diffraction patterns of the models were then simulated using the Diffraction-Crystal module.

Mechanical Characterization. Tensile tests were performed on seven solvent-cast green PNBT films at a crosshead

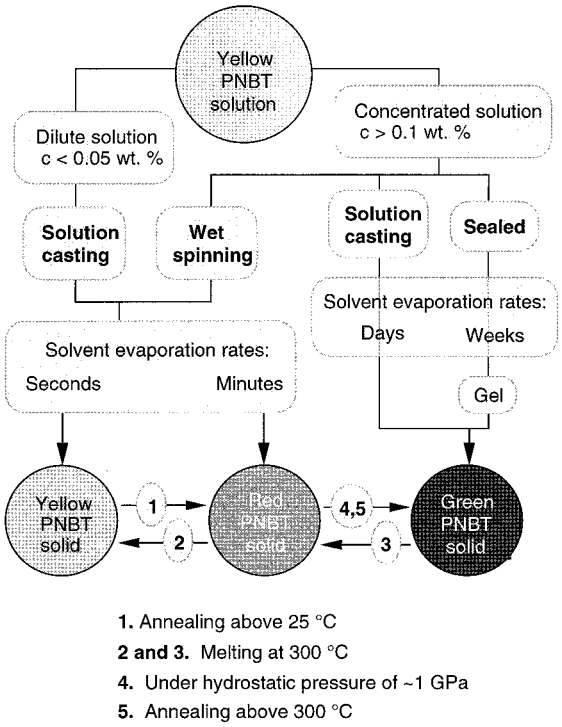

Figure 3. Processing chart for PNBT. Yellow, red, and metallic-green samples can be produced by varying parameters such as solution concentration, solvent evaporation rate, temperature, and pressure.

speed of 0.07 mm/min and a gauge length of 25.4 mm. The rectangular samples had a length of 36 mm, a width of 3 mm, and a thickness of 5−10 μm. Toe corrections of the stress−strain plots were performed as specified by ASTM standard test D882-91.[35] The elastic modulus was calculated by assuming all deformation up to 0.5% strain to be elastic.

3. Results

Chromism. The optical properties of PNBT films and fibers were found to be very sensitive to processing parameters. Variations in processing conditions such as polymer concentration, solvent evaporation rate, temperature, and pressure could produce yellow, red, or metallic-green specimens. Figure 3 shows the different processing schemes used in this study and their relationship to the observed sample color.

As-synthesized PNBT was deep red in color and dissolved into chloroform or toluene to form bright yellow solutions. These solutions were cast into films and fibers of different colors by varying their concentration and rate of solvent evaporation. For example, spin coating from dilute solution induced rapid solvent evaporation and yielded yellow films, while air-drying produced red ones. Very slow solvent evaporation rates were induced by partially enclosing 0.5 wt % polymer solutions and produced metallic-green films. During fiber spinning, the solvent evaporation rate varied according to the solvent used. Filaments spun from chloroform solutions dried quickly to form bright yellow fibers, while those spun from toluene solutions dried more slowly and became copper-red.

Dissolution of solid PNBT samples in chloroform or toluene resulted in photoluminescent yellow solutions (λ_{em} = 520 nm),[21] regardless of the color of the original solid sample. Adding small amounts of nonsolvent to the PNBT solutions decreased solubility and induced aggregation, as has been previously observed for

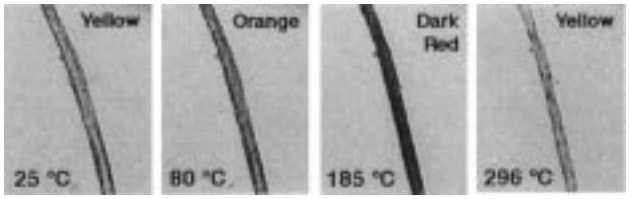

Figure 4. Thermochromic behavior of wet-spun yellow PNBT fibers monitored at 10 °C/min. Yellow samples gradually become red upon heating above 25 °C and revert back to yellow at approximately 300 °C.

P3ATs.[7,36] Increases in the polymer concentration caused solutions to become orange-yellow and led to a color change to purple-red after a period ranging from days to months. This process appeared to involve aggregation of the polymer chains and may include the phase separation of swollen polymer precipitates from the solution. Such PNBT "gels" dried to produce a flaky metallic-green solid. The formation of a gel phase has been reported by Prosa and Winokur to have a role in the formation of a secondary crystalline phase in P3ATs.[16] Gelation at high solution concentrations is a common phenomenon in lyotropic liquid crystals.[37]

Thermal treatment of PNBT films and fibers led to significant color changes in all of the samples studied. Thermochromic behavior varied according to the initial color of the sample and could involve both red shifts and blue shifts. Red and green PNBT samples showed a reversible blue shift at approximately 300 °C during which the samples became bright yellow. Yellow PNBT samples showed a gradual but irreversible red shift when heated above room temperature (Figure 4). Like drying solvent-cast films, the color of the samples changed from yellow to orange and finally red. Further heating of the then red samples also showed a blue shift at 300 °C. This latter blue shift was indistinguishable from that observed in other red or green PNBT samples and is quite similar to the order−disorder transitions observed in P3ATs.[4,9,10]

Red shifts of the optical absorption maximum occurred only on yellow samples and have been monitored by Nanos et al. through UV−vis spectroscopy.[21] These experiments revealed a sharp transition between two electronic species in which the species with the longer electron delocalization (λ_{max} = 527 nm) grew at the expense of the other (λ_{max} = 434 nm). After annealing a film for 4 h at 160 °C it appeared uniformly red, yet a fraction of the original yellow species remained in the form of a shoulder at λ_{max} = 434 nm. A similar color transition has been associated with the crystallization process of poly(3-dodecylthiophene).[38]

Applied pressures in the range of 1 GPa were found to induce permanent color changes on red bulk PNBT samples. The pressed samples were dark green and lacked the metallic appearance observed in cast or annealed green samples. Such piezochromism has also been observed in bulk red samples of poly(nonylbithiazole-*co*-ethynylene) (PENBT),[27] which become metallic-green under similar applied pressures. Since the polymer chains tend to align parallel to the plane of the substrate,[39] the applied pressure is expected to lead to closer π-stacking of thiazole rings between neighboring chains and increased planarity along the backbone.

Thermal Characterization. Red and green samples showed very similar thermal stability under nitrogen or air atmospheres, reaching a 5% weight loss at approximately 450 °C. DSC samples with no previous

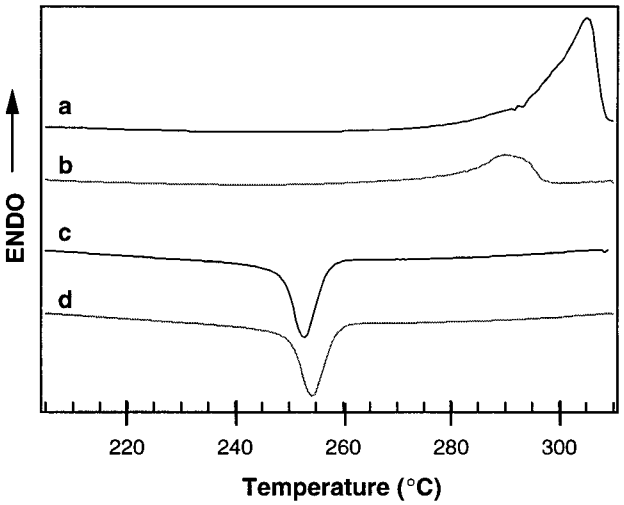

Figure 5. DSC thermograms of a red PNBT sample recorded at 10 °C/min. Traces a and b correspond to the first and second heating runs; traces c and d correspond to the first and second cooling runs. At the end of each heating cycle the samples were annealed at 310 °C for 5 min.

thermal history (i.e., tested as-synthesized or as-cast from solution) showed one endothermic peak upon heating at approximately 300 °C and one exothermic peak upon cooling at approximately 250 °C (Figure 5, Table 1). Subsequent DSC cycles of the samples showed a broad endothermic peak during heating at approximately 285 °C and a single exothermic peak during cooling at approximately 250 °C. A summary of these findings is listed in Table 1.

The endothermic transition observed during the initial heating cycle of PNBT at approximately 300 °C corresponds to the order−disorder transition previously observed by optical microscopy and has been identified as its melting point.[21] We have found that thermal treatment may suppress this phase transition in favor of a broader endothermic transition at approximately 285 °C. Annealing at 310 °C for 5 min triggered a color transition to green in yellow and red PNBT samples, and thus all specimens had become green by the end of their DSC cycles, regardless of their initial appearance.

Structural Characterization. Although the initial diffusion couple samples were optically isotropic, subsequent solvent evaporation led to the appearance of birefringent regions near the edge of the coverslip. Crystallization was evident at the solution−air boundaries in the form of well-defined regions of red polymer. Meanwhile, a liquid crystalline texture began to form between the isotropic and crystalline regions. Figure 6 shows the two phase boundaries as observed between crossed polarizers. It is interesting to note that observation of the samples without crossed polarizers showed a single well-defined boundary between the red crystalline solid and the yellow solution. These results are consistent with the contention that red color arises from crystalline order within the polymer, while yellow results from the increased torsion and chain twists present in both the isotropic and liquid crystalline regions. There are several reports on the thermotropic behavior of both regioregular and regioirregular poly(3-alkylthiophene)s (P3ATs);[15,40,41] mesophase formation has been proposed to mediate thermochromatic processes and the formation of different crystal phases in P3ATs.[10,16,40] Prosa et al. have observed the formation of a gellike phase in regioregular poly(3-octylthiophene) and poly(3-dodecylthiophene),[16] but we are not aware of any reports of lyotropic behavior in P3ATs.

The *d* spacings of different PNBT samples were measured using WAXS (Figure 7). Red and green PNBT samples showed sharp peaks at approximately 2.4, 1.2, 0.8, and 0.36 nm and an amorphous halo at 0.45 nm, while yellow samples showed a broad peak at 2.0 nm and an amorphous halo also at 0.45 nm (Table 2). The small-angle spacing of green (2.4 nm) and yellow (2.0 nm) films was confirmed through SAXS. Although red and green PNBT specimens had very similar *d* spacings, their average crystallite dimensions (ΔD) and degree of crystallinity (X_c) differed according to the processing scheme(s) used (Table 3). Crystal sizes ranging from approximately 5 to 30 nm and crystalline contents of roughly 20−70% were calculated though WAXS, compared to 7−20 nm and 10−23% for P3ATs.[10,15,17,42] Green solvent-cast samples had a large crystal size along (100) and a higher degree of crystallinity than red solvent-cast samples ($\Delta D_{100} = 10 \pm 2$ nm vs 6 ± 1 nm and $X_c = 60 \pm 35\%$ vs $44 \pm 14\%$, respectively). In contrast, green samples obtained through thermal annealing had a larger crystal size ($\Delta D_{100} = 29 \pm 4$ nm) but a lower degree of crystallinity ($22 \pm 1\%$) than solvent-cast red samples. Samples subjected to hydrostatic pressure saw a very slight increase in degree of crystallinity (from 34% to 37%) and no change in crystal size ($\Delta D_{100} = 7$ nm). Note that the 6 ± 1 nm crystal size calculated by WAXS for solvent-cast red PNBT is significantly smaller than the 13 ± 6 nm previously measured by low-dose high-resolution transmission electron microscopy (HRTEM).[39]

The X-ray and electron diffraction patterns of oriented fibers showed features similar to those observed in the powder WAXS data. X-ray diffraction photographs showed equatorial reflections at approximately 2.3 and 0.77 nm, a meridional reflection at 0.36 nm, and an amorphous halo at 0.47 nm (Figure 8a). Selected area electron diffraction (SAED) showed an equatorial reflection at 0.36 nm and an amorphous halo at 0.46 nm (Figure 8c).

Molecular Modeling. We have constructed a molecular model of PNBT based on experimental X-ray and electron diffraction data. The model, shown in Figure 9, has two trans planar chains with thiazole rings π-stacked onto rings of the opposite regiosymmetry (e.g., head over tail), allowing bulky sulfur atoms and alkyl side chains to stack on alternating sides. This mode of stacking is consistent with the absence of (001) reflections on the X-ray and ED fiber patterns and is further supported by current electron diffraction studies of PNBT single crystals, which we will report on separately. The simulated orthorhombic unit cell has two bithiazole units per cell and parameters of $a = 2.38$ nm, $b = 0.72$ nm, $c = 0.79$ nm, and $\rho = 1.023$ g/cm^3. X-ray and electron diffraction patterns of this model were calculated for different crystal size and fiber misorientation values; the best fits are shown in Figures 8 and 10. The most intense calculated reflections ($I > 5\%$) for both X-ray and electron fiber diffraction are listed in Table 4. According to these calculations, the four main WAXS peaks are (100), (200), (300), and (020), while the best fit between simulated and experimental data corresponds to crystal dimensions of 15 nm × 7 nm × 1 nm (Figure 10). Significant diffraction peaks were also calculated for (011) and (211), but these reflections overlap with the amorphous halo, and it is thus not clear

Table 1. Transition Heats and Temperatures of PNBT Samples Measured through Differential Scanning Calorimetry (DSC)

	transition temperatures (°C)				transition heats (J/g)			
	first cycle		second cycle		first cycle		second cycle	
sample	heating	cooling	heating	cooling	heating	cooling	heating	cooling
green PNBT	300 ± 2	246 ± 1	284 ± 1	245 ± 2	29 ± 1	−15 ± 3	8 ± 1	−14 ± 2
red PNBT	305 ± 1	249 ± 5	289 ± 2	249 ± 4	33 ± 4	−15 ± 5	11 ± 5	−15 ± 5
yellow PNBT	300 ± 1	252 ± 1	294 ± 10	252 ± 1	38 ± 11	−19 ± 2	17 ± 2	−20 ± 3

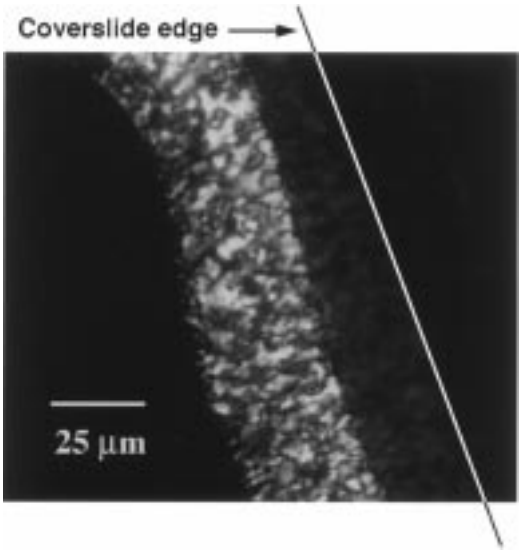

Figure 6. Edge of a PNBT diffusion couple between crossed polarizers as seen from above. The micrograph shows (from left to right) well-defined regions of isotropic, liquid crystalline, and crystalline textures.

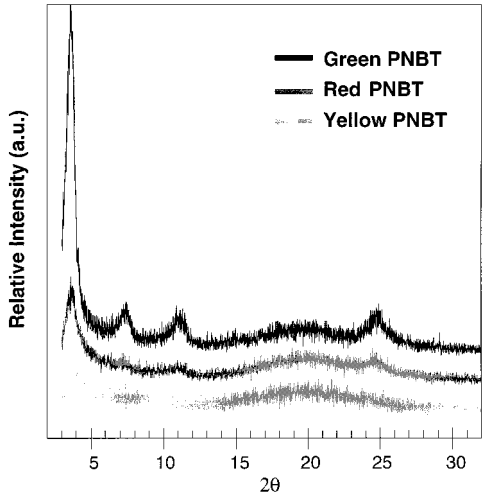

Figure 7. Wide-angle X-ray scattering (WAXS) patterns of green, red, and yellow PNBT samples.

Table 2. Correlation Distances (*d* Spacings, nm) of Yellow, Red, and Green PNBT Samples Measured by Wide-Angle X-ray Scattering (WAXS)

green PNBT	red PNBT	yellow PNBT
2.43 ± 0.3	2.36 ± 0.6	1.97
1.23 ± 0.2	1.24 ± 0.2	
0.82 ± 0.2	0.84 ± 0.2	
0.358 ± 0.03	0.361 ± 0.01	

whether they contribute to the experimental scattering profile. Simulated fiber X-ray diffraction patterns matched the experimental data with (100), (200), (300), and (020) equatorials and the pseudomeridional (202) reflection for crystal dimensions of 20 nm × 2 nm × 20 nm and a fiber misorientation (orientation half-width) of 15° (Figure 8b). The latter is an off-axis reflection that appears near the meridian due to fiber misorientation. Electron diffraction simulations of 10 nm × 6 nm × 20 nm crystals on a fiber misoriented by 15° matched the (211) and (202) off-axis reflections and the (020) equatorial (Figure 8d). Again, the (202) appears near the meridian due to fiber misorientation.

Table 3. Average Degree of Crystallinity (X_c) and Crystal Size along (100) (ΔD_{100}) for Red and Green PNBT Samples

color	processing method	X_c (%)	ΔD_{100} (nm)
red	solvent-cast	44 ± 14	6 ± 1
green	solvent-cast	60 ± 35	10 ± 2
green	annealed	22 ± 1	29 ± 4

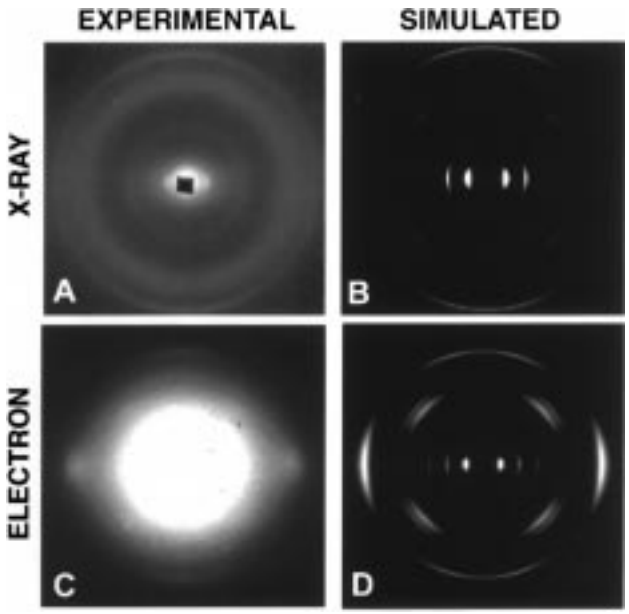

Figure 8. Experimental vs simulated X-ray and electron diffraction patterns of oriented PNBT samples.

Mechanical Characterization. The tensile properties of green PNBT have been found to be comparable to those of P3ATs. The average tensile modulus was 151 MPa, the stress at break was 4 MPa, and the elongation of green PNBT films was 7% (Table 5). Figure 11 shows a comparison between the modulus (E) and the stress at break (σ_b) of PNBT and P3ATs as a function of side chain length. Interpolation of the data available for poly(3-octylthiophene) and poly(3-decylthiophene) indicates that PNBT has a higher modulus but a somewhat lower strength at break than that expected for poly(3-nonylthiophene).[8,17] The higher modulus is consistent with the more planar structure projected for regioregular PNBT.[8,17,21]

4. Discussion

Chromism. The observed relationship between color changes and processing conditions indicates that red

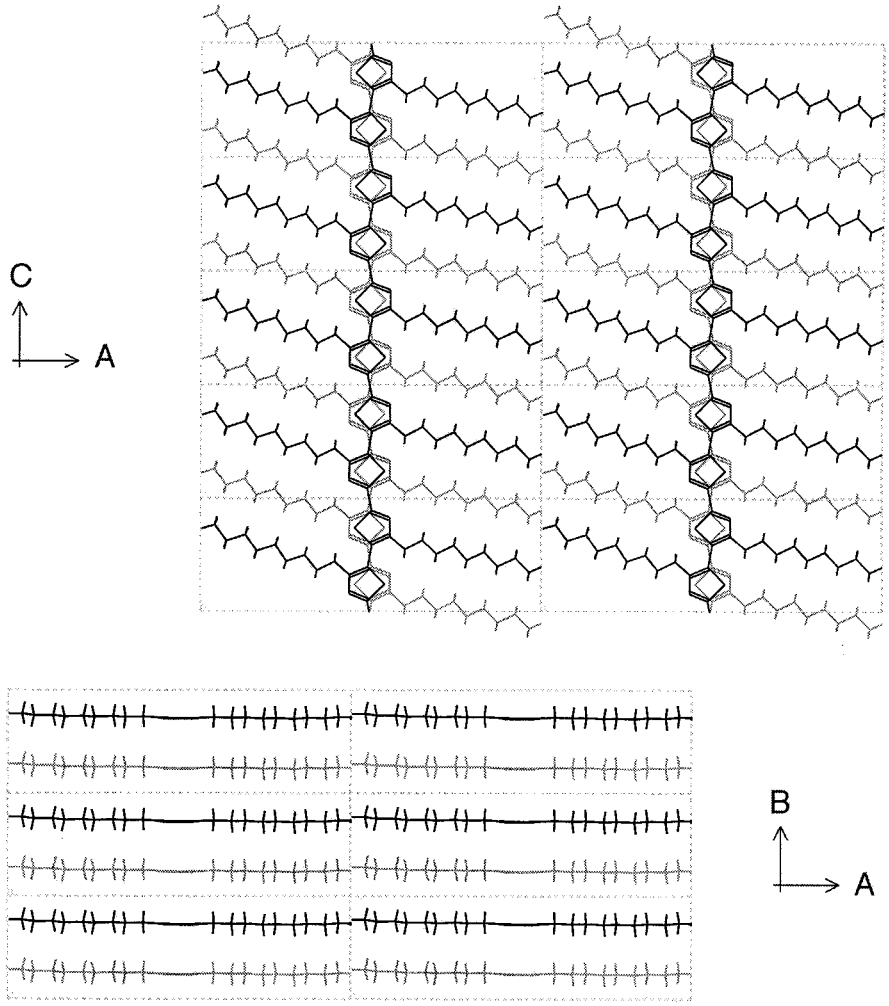

Figure 9. Molecular model of PNBT. Top: view along the *b*-axis. Bottom: view along the *c*-axis. The simulated orthorhombic unit cell dimensions are $a = 2.38$ nm, $b = 0.72$ nm, $c = 0.79$ nm, and $\rho = 1.023$ g/cm^3.

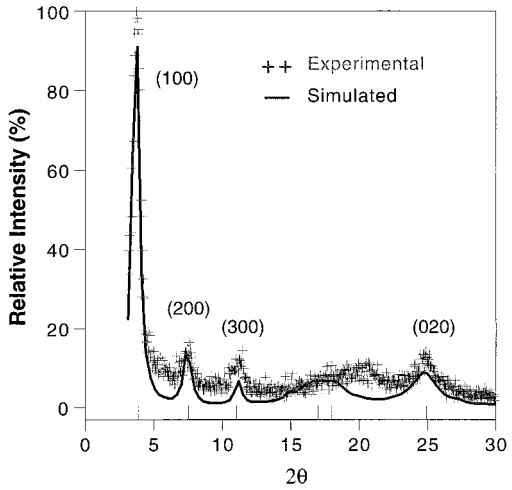

Figure 10. Experimental vs simulated WAXS of green PNBT. The simulated crystal size is 15 nm × 7 nm × 1 nm.

and green PNBT result from processing schemes that increase the crystallinity of the material, whereas yellow PNBT results from schemes that diminish it. Thermal and solvent annealing changed the color of films and fibers from yellow to red or green and from red to green. X-ray diffraction confirmed that red and green samples are semicrystalline while yellow samples lack three-dimensional order. Indeed, the yellow PNBT films (λ_{abs} = 434 nm) show absorption characteristics similar to those of the dilute solution (λ_{abs} = 429 nm), indicating limited electron delocalization possibly due to a high concentration of torsional defects on the polymer backbone.[7,20] On the other hand, the absorption maxima of red (λ_{abs} = 527 nm) and green PNBT samples (λ_{abs} = 527 and 619 nm) showed red shifts with respect to yellow samples, indicating smaller band gaps. These samples are expected to have a larger degree of backbone planarity.

Thermal Characterization. The thermal behavior of yellow, red, and green PNBT samples was found to be very similar. Microstructural changes occurred after the first heating and cooling cycles, as indicated by a color change, a new endothermic transition at about 285 °C, the absence of a transition at 300 °C, and a significant increase in the average crystal size calculated by WAXS. The observed increases in crystal size are expected to be accompanied by increases in the melting temperature and would thus explain the absence of an endothermic transition at 300 °C. In that case, the emergence of a transition at 285 °C may be attributed to a liquid crystalline transition. We are currently investigating this possibility by means of optical microscopy.

Structural Characterization. WAXS data for the different PNBT samples indicate that red and green samples have the same crystal structure, although they differed in their degree of crystallinity and average

Table 4. Calculated X-ray (WAXS) and Electron Diffraction (ED) *d* Spacings of PNBT

WAXS powder				WAXS fiber				ED fiber			
d_{obs} (nm)	d_{calc} (nm)	*hkl*	I_{calc} (%)	d_{obs} (nm)	d_{calc} (nm)	*hkl*	I_{calc} (%)	d_{obs} (nm)	d_{calc} (nm)	*hkl*	I_{calc} (%)
2.43	2.38	100	100.0	2.26	2.38	100	57.9		2.38	100	9.4
1.23	1.19	200	15.3	1.14	1.19	200	27.4		1.19	200	5.6
0.82	0.79	300	5.9	0.77	0.79	300	15.8		0.79	300	5.4
	0.53	011	27.3		0.53	011	74.1		0.53	011	41.7
	0.49	211	10.5		0.49	211	28.9	0.48	0.49	211	19.4
	0.38	202	5.3		0.39	102	9.2	0.37	0.38	202	13.5
0.36	0.36	020	17.3	0.36	0.38	202	46.4	0.36	0.36	020	100.0
				0.36	0.36	020	100.0		0.36	120	14.6
					0.36	120	19.8		0.35	220	8.4
					0.35	220	11.6		0.33	320	7.5
					0.33	320	8.9		0.26	222	16.0
					0.26	222	15.9				

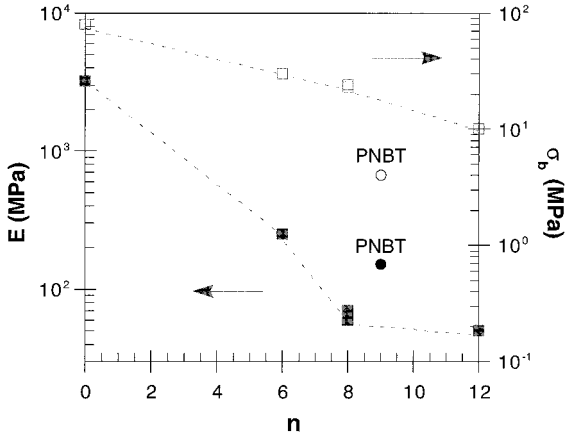

Figure 11. Modulus and elongation at break of PNBT (●) and poly(3-alkylthiophene)s (P3ATs) (■) as a function of alkyl chain length. Points $n = 0$, 6, 8, and 12 are taken from refs 8 and 17.

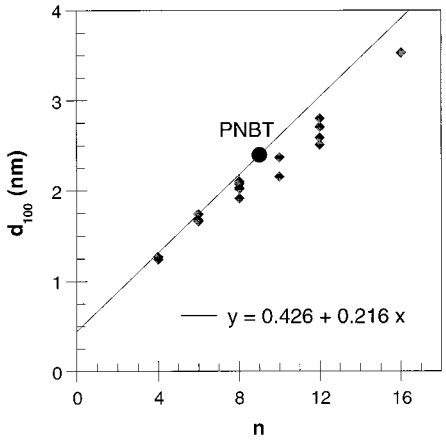

Figure 12. Side chain spacing of PNBT (●) and P3ATs (◆) as a function of alkyl chain length. Points $n = 4-8$ and 10−16 are taken from refs 8−10, 15−17, 40, and 43−45.

Table 5. Tensile Modulus (*E*), Stress at Break (σ_b), and Strain (ϵ) of Green PNBT Films

σ_y (MPa)	*E* (MPa)	σ_b (MPa)	ϵ (%)
0.79 ± 0.25	151 ± 27	4 ± 1	7.0 ± 3.4

crystal size. The first peak observed in all samples is attributed to the correlation distance between polymer backbones, or d_{100}, which is determined by the size and conformation of the alkyl side chains (Figure 9). This interpretation is consistent with a P3AT model proposed by Thémans et al. in which the thiophene rings are arranged in a trans conformation and the side chains form an angle of ∼58° with the axis of the planar backbone.[43] The model reasonably predicts d_{100} for butyl-, hexyl-, and octyl-substituted polythiophenes but overestimates the *d* spacings of P3ATs whose side chains are longer than octyl, presumably due to increased side chain disorder (Figure 12).[8−10,15−17,40,42−44] Similarly, the predicted value of 2.39 nm for a nonyl-substituted polythiophene closely agrees with the d_{100} of green and red PNBT samples but overestimates the *d* spacing of yellow specimens.

The second and third WAXS peaks are attributed to higher order reflections of the first peak, or (200) and (300), as has been done for P3ATs.[9,10] In PNBT, the third peak may also correspond to the correlation distance of the bithiazole repeat unit, (001). However, electron and X-ray diffraction patterns of PNBT fiber indicate that this 0.8 nm peak is an equatorial reflection, whereas (001) would be a meridional. The fourth WAXS peak is attributed to the $\pi-\pi$ stacking distance between aromatic groups in adjacent chains. In P3ATs, this interchain reflection has been reported to range from 0.38 to 0.4 nm, slightly larger than the 0.36 nm observed in PNBT.[9,10,15,17,42]

Although the average crystal size and degree of crystallization of PNBT samples varied widely depending on the processing parameters used, green PNBT samples were generally more crystalline and/or had larger crystals than red samples. The combined changes in crystallinity and crystal dimensions might be better expressed as an average intercrystallite distance which would decrease with an intensification of optical absorption, and hence reflection, of the sample. Though ΔD_{100} is expected to have a negligible impact on charge transport properties, its variations could reflect a change in overall crystal size that cannot be accurately measured by means of WAXS. Previous analyses of the optical properties of PNBT samples by Nanos et al. have suggested that green PNBT crystals are longer and more ordered along the *b* axis than red PNBT crystals.[21]

Our data show how subtle variations in the structure of PNBT can give rise to changes in apparent color. Small structural variations have been previously observed to cause dramatic changes on films of alkanethiol-coated silver particles, including a sharp transition to a metallic sheen.[45] These optical transitions do not require changes in crystal symmetry but only small changes in the average interparticle separation induced by lateral compression of the films.

Molecular Modeling. The calculated X-ray and electron diffraction patterns of our PNBT model provided reasonable fits of the peak positions and relative intensities of the available experimental data. The best fits between simulated and experimental diffraction data were obtained by using anisotropic crystal dimen-

sions. In the case of both X-ray and ED fiber patterns, the best fit was obtained by simulating crystals that were shorter along the *b*-axis, whereas in the case of powder WAXS the simulated crystal was shortest along the *c*-direction and longest along the *a*-axis. These relative dimensions are consistent with the greater main-chain orientation induced by fiber spinning as compared to solvent casting. The (020) equatorial reflection, which corresponds to the $\pi-\pi$ stacking correlation distance, was significantly weaker in the WAXS fiber patterns than in the ED fiber patterns. This is likely due to the latter samples being thermally annealed, whereas the wet-spun fibers used for X-ray were tested as-spun.

The general features of our model are similar to those proposed by Prosa et al. for P3ATs: backbone planarity, tilted packing of the alkyl chains, and a lack of side chain interdigitation.[16] The model is also somewhat similar to those proposed for P3HT and P3OT by Mårdalen et al., in which the conjugated chains stack staggered along the backbone axis.[17]

5. Conclusions

The electronic structure of PNBT was found to be very sensitive to processing conditions. Changes in polymer concentration, solvent evaporation rate, temperature, and pressure yielded samples of various colors. The effective conjugation length of the samples varied with their degree of crystallinity; yellow samples were found to be only weakly ordered, while red and green samples were semicrystalline. Red and green specimens had similar crystal structures, although green samples had a higher degree of crystallinity and/or a larger average crystal size in the [100] direction. This combination of changes might indicate a difference in intercrystallite spacing, where the smaller spacing would correlate with an intensification of optical absorption and hence reflection. The side-to-side distance between polymer backbones was somewhat larger than would be expected for a nonyl-substituted P3AT while the $\pi-\pi$ stacking distance was somewhat smaller, indicating increased backbone planarity in PNBT. This is consistent with PNBT's larger tensile modulus as compared to that of P3ATs. A planar, all-trans molecular model was found to provide a reasonable fit to the experimental X-ray and electron diffraction data.

Acknowledgment. The authors are grateful to Anthony H. Francis for helpful discussions and Jo A. Johnson for her help in synthesizing the PNBT used in this study. This work was supported by the University of Michigan Display Technology and Manufacturing Center and the National Science Foundation (DMR-9707975, DMR-9510274, and NYI Award DMR-9257569). L.G.R. thanks the University of Michigan Rackham School of Graduate Studies for fellowship support.

References and Notes

(1) Braun, D.; Gustafsson, G.; McBranch, D.; Heeger, A. J. *J. Appl. Phys.* **1992**, *72* (2), 564.
(2) Garnier, F.; Hajlaoui, R.; Yassar, A.; Srivastava, P. *Science* **1994**, *265*, 1684.
(3) Bidan, G. *Sens. Actuators, B* **1992**, *6*, 45.
(4) Inganäs O. *Trends Polym. Sci.* **1994**, *2* (6), 189.
(5) Yoshino, K.; Nakajima, S.; Onoda, M.; Sugimoto, R. *Synth. Met.* **1989**, *28* (C), 349.
(6) Yoshino, K.; Nakao, K.; Onoda, M.; Sugimoto, R. *Solid State Commun.* **1988**, *68*, 513.
(7) Inganäs, O.; Salaneck, W. R.; Österholm, J.-E.; Laakso, J. *Synth. Met.* **1988**, *22*, 395.
(8) Moulton, J.; Smith, P. *Polymer* **1992**, *33*, 2340.
(9) Chen, S.-A.; Ni, J.-M. *Macromolecules* **1992**, *25*, 6081.
(10) Yang, C.; Orfino, F. P.; Holdcroft, S. *Macromolecules* **1996**, *29*, 6510.
(11) McCullough, R. D.; Lowe, R. D. *J. Chem. Soc., Chem. Commun.* **1992**, *1*, 70.
(12) Chen, T.-A.; Wu, X.; Rieke, R. D. *J. Am. Chem. Soc.* **1995**, *117*, 233.
(13) Meille, S. V.; Farina, A.; Bezziccheri, F.; Gallazzi, M. C. *Adv. Mater.* **1994**, *6*, 848.
(14) Mårdalen, J.; Fell, H. J.; Samuelsen, E. J.; Bakken, E.; Carlsen, P. H. J.; Andersson, M. R. *Macromol. Chem. Phys.* **1985**, *196*, 553.
(15) Winokur, M. J.; Spiegel, D.; Kim, Y.; Hotta, S.; Heeger, A. J. *Synth. Met.* **1989**, *28* (C), 419.
(16) Prosa, T. J.; Winokur, M. J.; McCullough, R. D. *Macromolecules* **1996**, *29*, 3654.
(17) Mårdalen, J.; Samuelsen, E. J.; Gautun, O. R.; Carlsen, P. H. *Synth. Met.* **1992**, *48*, 363.
(18) Salaneck, W. R.; Inganäs, O.; Thémans, B.; Nilsson, J. O.; Sjögren, B.; Österholm, J.-E.; Brédas, J.-L.; Svensson, S. *J. Chem. Phys.* **1988**, *89* (8), 4613.
(19) Salaneck, W. R. *Contemp. Phys.* **1989**, *30* (6), 403.
(20) Brédas, J. L.; Street, G. B.; Thémans, B.; André, J. M. *J. Chem. Phys.* **1985**, *383* (3), 1323.
(21) Nanos, J. I.; Kampf, J. W.; Curtis, M. D.; Gonzalez, L.; Martin, D. C. *Chem. Mater.* **1995**, *7*, 2232.
(22) Yamamoto, T.; Suganuma, H.; Maruyama, T.; Kubota, K. *J. Chem. Soc., Chem. Commun.* **1995**, *5*, 1613.
(23) Yamamoto, T.; Suganuma, H.; Maruyama, T.; Inoue, T.; Muramatsu, Y.; Arai, M.; Komarudin, D.; Ooba, N.; Tomaru, S.; Sasaki, S.; Kubota, K. *Chem. Mater.* **1997**, *9*, 1217.
(24) Curtis, M. D.; Cheng, H.; Nanos, J. I.; Nazri, G.-A. *Macromolecules* **1998**, *31*, 205.
(25) Politis, J. K.; Curtis, M. D.; Gonzalez, L.; Martin, D. C.; He, Y.; Kanicki, J. *Chem. Mater.* **1998**, *10*, 1713.
(26) Curtis, M. D.; Cheng, H.; Johnson, J. A.; Nanos, J. I.; Kasim, R.; Elsenbaumer, R. L.; Gonzalez Ronda, L.; Martin, D. C. *Chem. Mater.* **1998**, *10*, 13.
(27) He, Y.; Politis, J. K.; Cheng, H.; Curtis, M. D.; Kanicki, J. *IEEE Trans. Electron Devices* **1997**, *44* (8), 1282.
(28) Doshi, J.; Reneker, D. H. *J. Electrostat.* **1995**, *35*, 151.
(29) Meier, G.; Sackmann, E.; Grabmaier, J. G. *Applications of Liquid Crystals*; Springer-Verlag: New York, 1975.
(30) Kerkam, K.; Viney, C.; Kaplan, D.; Lombardi, S. *Nature* **1991**, *349*, 596.
(31) WaveMetrics Inc., Igor Pro, Version 2.02, 1994.
(32) Baltá-Calleja, F. J.; Vonk, C. G. *X-Ray Scattering of Synthetic Polymers*; Elsevier Science Publishers: Amsterdam, The Netherlands, 1989.
(33) Molecular Simulations Inc., Cerius^2 Molecular Modelling Software, Version 2.0, 1995.
(34) Mayo, S. L.; Olafson, B. D.; Goddard, W. A. *J. Phys. Chem.* **1990**, *94*, 8897.
(35) American Society for Testing and Materials, *ASTM Standards* **1991**, *D882−91*.
(36) Zerbi, G.; Chierichetti, B.; Inganäs, O. *J. Chem. Phys.* **1991**, *94* (6), 4646.
(37) Hiltrop, K. In *Liquid Crystals*; Stegemeyer, H., Ed.; Springer-Verlag: New York, 1994.
(38) Park, K. C.; Levon, K. *Macromolecules* **1997**, *30*, 3175.
(39) González Ronda, L.; Martin, D. C. *Macromolecules* **1997**, *30*, 1524.
(40) Bolognesi, A.; Porzio, W.; Provasoli, F.; Ezquerra, T. *Makromol. Chem.* **1993**, *194*, 817.
(41) Faïd, K.; Fréchette, M.; Ranger, M.; Mazerolle, L.; Lévesque, I.; Leclerc, M. *Chem. Mater.* **1995**, *7*, 1390.
(42) Collier, C. P.; Saykally, R. J.; Shiang, J. J.; Henrichs, S. E.; Heath, J. R. *Science* **1997**, *277*, 1978.
(43) Thémans, B.; Salaneck, W. R.; Brédas, J. L. *Synth. Met.* **1989**, *28* (C), 359.
(44) Gustafsson, G.; Inganäs, O.; Österholm, H.; Laakso, J. *Polymer* **1991**, *32*, 1574.
(45) Tashiro, K.; Ono, K.; Minagawa, Y.; Kobayashi, K.; Kawai, T.; Yoshino, K. *J. Polym. Sci., Part B: Polym. Phys.* **1991**, *29*, 1223.

MA990057+